

Multiple magnon modes in the $\text{Co}_3\text{Sn}_2\text{S}_2$ Weyl semimetal candidate

O.O. Shvetsov,¹ V.D. Esin,¹ A.V. Timonina,¹ N.N. Kolesnikov,¹ and E.V. Deviatov¹

¹*Institute of Solid State Physics of the Russian Academy of Sciences, Chernogolovka, Moscow District, 2 Academician Ossipyan str., 142432 Russia*

(Dated: April 17, 2019)

We experimentally investigate electron transport in kagome-lattice ferromagnet $\text{Co}_3\text{Sn}_2\text{S}_2$, which is regarded as a time reversal symmetry broken Weyl semimetal candidate. We demonstrate $dV/dI(I)$ curves with pronounced asymmetric dV/dI spikes, similar to those attributed to current-induced spin-wave excitations in ferromagnetic multilayers. In contrast to multilayers, we observe several dV/dI spikes' sequences at low, $\approx 10^4$ A/cm², current densities for a thick single-crystal $\text{Co}_3\text{Sn}_2\text{S}_2$ flake in the regime of fully spin-polarized bulk. The observed behavior necessarily requires a distinct magnetic structure with a small total spin value, so we attribute dV/dI spikes to multiple magnon branches in $\text{Co}_3\text{Sn}_2\text{S}_2$ Weyl surface states. We demonstrate splitting of the magnon branches in high magnetic fields, which may reflect reconstruction of spin textures in the surface state due to the spin-momentum locking. Presence of spin-transfer effects at low current densities in $\text{Co}_3\text{Sn}_2\text{S}_2$ makes the material attractive for applications in spintronics.

PACS numbers: 73.40.Qv 71.30.+h

I. INTRODUCTION

A strong area of interest in condensed matter physics is topological semimetals¹. Dirac semimetals host the 4-fold degenerate topologically protected Dirac points, which are the special points of Brillouin zone with three dimensional linear dispersion. In Weyl semimetals (WSM), by breaking time reversal or inversion symmetries, the 4-fold degeneration of Dirac points declines to the 2-fold one, so every Dirac point splits into two Weyl nodes with opposite chiralities. Similarly to topological insulators and quantum Hall insulators, Weyl semimetals have topologically protected surface states, which are Fermi arcs connecting projections of Weyl nodes on the surface Brillouin zone¹. First experimentally investigated WSMs were non-centrosymmetric crystals with broken inversion symmetry. Spin- and angle- resolved photoemission spectroscopy (SARPES) data indeed demonstrate spin-polarized surface Fermi arcs^{2,3}.

Also, ferromagnetic and antiferromagnetic WSMs with broken time-reversal symmetry can be discussed¹. There are only a few candidates of magnetically ordered materials for the realization of WSMs⁴⁻⁷. Recently, giant anomalous Hall effect was reported^{8,9} for the kagome-lattice ferromagnet $\text{Co}_3\text{Sn}_2\text{S}_2$, as an indication for the existence of a magnetic Weyl phase. Fermi arcs were also visualized¹⁰ for $\text{Co}_3\text{Sn}_2\text{S}_2$ by scanning tunneling spectroscopy.

The anomalous Hall effect (AHE) appears in a large class of magnetically ordered materials. It manifests itself as an anomalous Hall conductance in zero magnetic field. AHE is known due to the two qualitatively different microscopic mechanisms: extrinsic processes due to scattering effects, and an intrinsic mechanism connected to the Berry curvature¹¹⁻¹³. The latter variant is realized for WSMs, where the Berry curvature is enhanced at Weyl nodes¹. Thus, an intrinsic large anomalous Hall conductivity is the specifics of time reversal symmetry

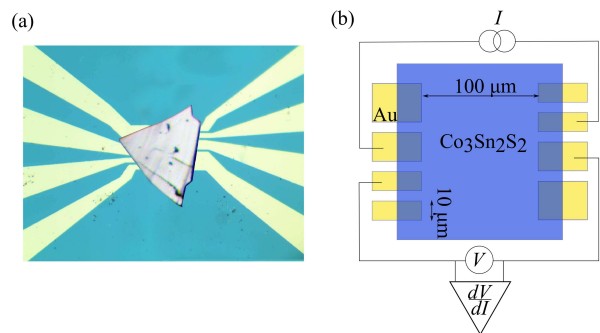


FIG. 1. (Color online) (a) A top-view image of the sample. A flat (about 100 μm size and 1 μm thick) single-crystal $\text{Co}_3\text{Sn}_2\text{S}_2$ flake is weakly pressed on the insulating SiO_2 substrate with 100 nm thick, 5 μm separated gold leads. The leads are of 40 μm , 20 μm , 10 μm and 10 μm width from up to down for the left side of the sample. (b) The sketch of a sample with electrical connections. Non-linear $dV/dI(I)$ curves are measured by a standard four-point technique, so a large dc current I is additionally modulated by a low ac component.

broken WSMs^{8,9}.

Another specifics of the magnetically ordered materials is the possibility of spin-wave excitations. Current-induced excitation of spin waves, or magnons, was demonstrated in spin valves at large electrical current densities²⁰⁻²⁶. The spin valves are the sandwich structures, where spin-dependent scattering affects the magnetic moments of two spin-polarized layers, while their mutual orientation defines the differential resistance. In low external magnetic fields, the spin-polarized current flowing from the free layer to the static layer transfers part of its spin angular momentum, and the magnetization of the free layer can be switched antiparallel to the static layer. On the contrary, the inverse current produces a switch back to the parallel orientation. In the

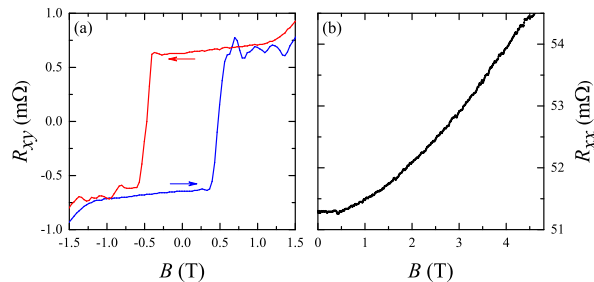


FIG. 2. (Color online) (a) Giant anomalous Hall effect, which confirms⁸ high quality of our kagome-lattice semimetal $\text{Co}_3\text{Sn}_2\text{S}_2$ samples^{8,9}. The Hall resistance R_{xy} demonstrates hysteresis behavior and sharp switchings at ≈ 0.5 T. Arrows indicate the scanning directions. (b) Positive, non-saturating longitudinal magnetoresistance in normal magnetic field, which is a hallmark of compensated semimetals^{8,9}. The measurements are performed at 4.2 K.

high-field regime, the spin-transfer effect does not lead to a full magnetization reversal, but precessing spin-wave excitations take place instead in between parallel and antiparallel alignment. The precession is observed only for one current polarity and is presented as a sharp peak in differential resistance^{20–26}. Electric field assisted magnetization dynamics was also predicted^{14,15} for WSMs, which requires experimental investigations.

Here, we experimentally investigate electron transport in kagome-lattice ferromagnet $\text{Co}_3\text{Sn}_2\text{S}_2$, which is regarded as a time reversal symmetry broken Weyl semimetal candidate. We demonstrate $dV/dI(I)$ curves with pronounced asymmetric dV/dI spikes, similar to those attributed to current-induced spin-wave excitations in ferromagnetic multilayers. In contrast to multilayers, we observe several dV/dI spikes' sequences at low, $\approx 10^4$ A/cm², current densities for a thick single-crystal $\text{Co}_3\text{Sn}_2\text{S}_2$ flake in the regime of fully spin-polarized bulk. The observed behavior necessarily requires a distinct magnetic structure with a small total spin value, so we attribute dV/dI spikes to multiple magnon branches in $\text{Co}_3\text{Sn}_2\text{S}_2$ Weyl surface states. We demonstrate splitting of the magnon branches in high magnetic fields, which may reflect reconstruction of spin textures in the surface state due to the spin-momentum locking. Presence of spin-transfer effects at low current densities in $\text{Co}_3\text{Sn}_2\text{S}_2$ makes the material attractive for applications in spintronics.

II. SAMPLES AND TECHNIQUE

$\text{Co}_3\text{Sn}_2\text{S}_2$ single crystals were grown by the gradient freezing method. Initial load of high-purity elements taken in stoichiometric ratio was slowly heated up to 920° C in the horizontally positioned evacuated silica ampoule, held for 20 h and then cooled with the furnace to the ambient temperature at the rate of 20 deg/h. The

obtained ingot was cleaved in the middle part. The Laue patterns confirm the hexagonal structure with (0001) as cleavage plane. Electron probe microanalysis of cleaved surfaces and X-ray diffractometry of powdered samples confirmed stoichiometric composition of the crystal.

Despite it is possible to form contacts directly on the cleaved $\text{Co}_3\text{Sn}_2\text{S}_2$ crystal plane, large samples are not suitable for transport experiments: it is impossible to create high current density in a thick sample, which is crucial for the current-induced magnetization experiments.

Instead, the leads pattern is formed on the insulating SiO_2 substrate by lift-off technique after thermal evaporation of 100 nm Au. The gold leads are separated by 5 μm intervals, see Fig. 1 (a), and (b). Since the kagome-lattice ferromagnet $\text{Co}_3\text{Sn}_2\text{S}_2$ can be easily cleaved along (0001) crystal plane, small (about 100 μm size and 1 μm thick) $\text{Co}_3\text{Sn}_2\text{S}_2$ flakes are obtained by a mechanical cleaving method. Then we select the most plane-parallel flakes with clean surface, where no surface defects could be resolved with optical microscope. They are transferred to the Au leads pattern and pressed slightly with another oxidized silicon substrate. A special metallic frame allows us to keep the substrates parallel and apply a weak pressure to the sample. No external pressure is needed for a $\text{Co}_3\text{Sn}_2\text{S}_2$ flake to hold on to a substrate with Au leads afterward^{16–18}.

We check by standard magnetoresistance measurements that our $\text{Co}_3\text{Sn}_2\text{S}_2$ flakes demonstrate giant anomalous Hall effect^{11–13} in normal to the flake's plane magnetic field. Fig. 2 (a) shows hysteresis behavior and sharp switchings in Hall resistance R_{xy} , the switchings' positions ≈ 0.5 T even quantitatively coincide with the previously reported ones^{8,9}. Fig. 2 (b) shows positive, non-saturating longitudinal magnetoresistance, which is also consistent with the reported behavior⁸ for $\text{Co}_3\text{Sn}_2\text{S}_2$ semimetal. Thus, magnetoresistance measurements confirms high quality of our $\text{Co}_3\text{Sn}_2\text{S}_2$ samples.

We study electron transport along the $\text{Co}_3\text{Sn}_2\text{S}_2$ surface by a standard four-point technique. The principal circuit diagram is depicted in Fig. 1 (b). To obtain $dV/dI(I)$ characteristics, a large (up to 3 mA) dc current I is additionally modulated by a low (≈ 5 μA) ac component. We measure both dc (V) and ac ($\sim dV/dI$) components of the voltage drop in Fig. 1 (b) with a dc voltmeter and a lock-in, respectively, after a broad-band preamplifier. The lock-in signal is checked to be independent of the modulation frequency. The obtained $dV/dI(I)$ curves are qualitatively independent on the particular choice of current and voltage probes.

The measurements are performed in a usual He4 cryostat equipped with a superconducting solenoid. $\text{Co}_3\text{Sn}_2\text{S}_2$ magnetic properties arise from the kagome-lattice cobalt planes, whose magnetic moments order ferromagnetically⁸ out of plane below 175 K. We do not see noticeable temperature dependence in the interval 1.4–4.2 K, so all the results below are obtained at 4.2 K.

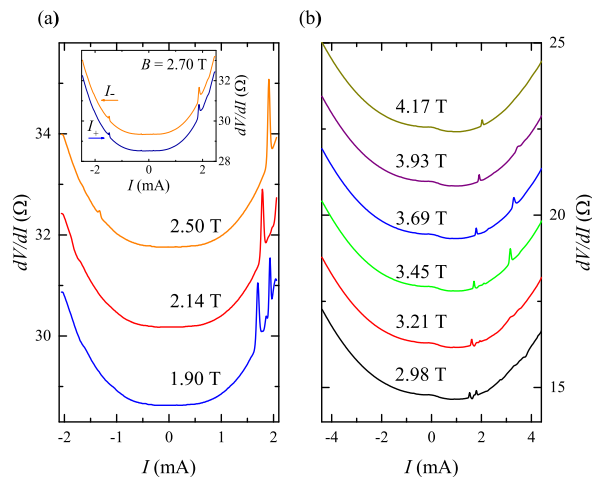


FIG. 3. Examples of $dV/dI(I)$ characteristics for two different samples, (a) and (b), respectively. The curves are shifted upward for clarity. dV/dI is rising with both bias current polarities without any saturation at high biases. There are well-developed dV/dI spikes for certain (positive) current polarity, their positions are sensitive to the magnetic field. The inset to (a) demonstrates a lack of hysteresis for different current sweep directions. The magnetic field is perpendicular to the flake's plane. The measurements are performed at 4.2 K.

III. EXPERIMENTAL RESULTS

Examples of $dV/dI(I)$ characteristics are shown in Fig. 3 (a) and (b). The curves demonstrate clear non-Ohmic behavior: dV/dI is rising with both bias current polarities without any saturation at high biases. This behavior is inconsistent with trivial reasons like tunneling through different sample defects, which generally leads to decreasing $dV/dI(I)$. Moreover, the experimental $dV/dI(I)$ curves are well reproducible for different samples with very different zero-bias resistance, cp. Fig. 3 (a) and (b). On the other hand, an overall symmetric increase in dV/dI is usually attributed to electron scattering in the magnetically ordered materials^{19,20}.

For the curves in Fig. 3 we observe well-developed dV/dI spikes for certain (positive) current polarity. These dV/dI features are well reproducible in different cooling cycles. The spike position is sensitive to the magnetic field, as depicted in Fig. 3, it moves to higher currents with increasing the magnetic field. In the same time, there is no noticeable hysteresis with the current sweep direction, see the inset to Fig. 3 (a). This behavior is very similar to one reported for ferromagnetic multilayers^{20–26}, where the dV/dI spikes have been attributed to spin-wave excitation modes.

In addition, small spikes are sometimes present at the counter (negative) current polarity, as it is depicted in Fig. 3 (a) for $B = 2.5$ T and for $B = 2.7$ T in the inset. These minor spikes have qualitatively the same magnetic field behavior, so we regard only the major ones at posi-

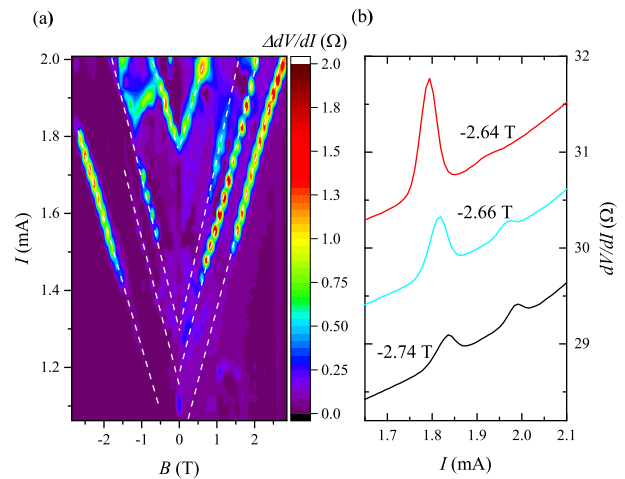


FIG. 4. (a) Evolution of dV/dI spikes' positions with magnetic field. The monotonous $dV/dI(I)$ is subtracted from the data, the colors correspond only to the spikes' amplitudes. There are several excitation branches with the linear field dependence, which are highlighted by white dashed lines. The slopes coincide within experimental accuracy, but the spikes vanish and reappear in some regions of the map. (b) An example of splitting of a particular branch in high magnetic fields, the curves are shifted downward for clarity. While the amplitude of one spike is decreasing, the other spike is emerging at higher current, see also the corresponding region in (a).

tive currents below.

The colormap in Fig. 4 (a) demonstrates evolution of dV/dI spikes with magnetic field, which is applied normally to the $\text{Co}_3\text{Sn}_2\text{S}_2$ flake. Since the general $dV/dI(I)$ shape is practically independent of the magnetic field, see Fig. 3, it is subtracted from the data. Thus, the colors correspond only to the spikes' amplitudes in Fig. 4 (a).

It is clear, that the dV/dI spikes' positions depend linearly on the magnetic field, as it has been also demonstrated^{20–26} for magnons²³ in multilayers. In contrast to multilayers, we observe several excitation branches, which are highlighted by white dashed lines on the colormap. The line slopes coincide within experimental accuracy, they also independent of the field direction. The spikes are better visible at highest currents, where they can be demonstrated even in zero magnetic field.

On the other hand, the relative amplitudes of the spikes are different for different branches, the spikes even vanish and reappear in some regions of the map. Also, we observe splitting of a particular branch in high magnetic fields, see also Fig. 4 (b): while increasing the magnetic field, the spike's amplitude is diminishing, an additional spike appears at different current position; in higher fields, two spikes coexist, see Fig. 4 (b). Such interplay generally reflects the ground state reconstruction^{27–29}.

IV. DISCUSSION

$dV/dI(I)$ curves with an overall symmetric increase in dV/dI and asymmetric dV/dI spikes have been reported for spin valves, i.e. for ferromagnetic multilayers²⁰⁻²⁶. In low magnetic fields, the hysteresis in $dV/dI(I)$ curves indicates current-induced switching in the orientation of layers' magnetic moments between parallel and antiparallel orientations. In the high-field regime, the high-bias dV/dI spikes correspond to a precessing spin-wave state with increasing deviations from the parallel alignment, which leads to increases in dV/dI resistance. At large external magnetic fields H , the critical current I_{sw} is given²³ by the Slonczewski model³⁰: $I_{sw} \sim S(H - H_{ex} + H_{an})$, where H_{ex} and H_{an} are the exchange and the anisotropy fields, respectively, S is the total spin for the magnetic layer. In experiments on multilayers²⁰⁻²⁶, the spin-wave excitation is characterized by injection of extremely high (10^9 A/cm²) current density for thin, 2-4 nm, Co layers.

We observe qualitatively similar effects in bulk properties of single-crystal Co₃Sn₂S₂ flakes. In this case, there is no separate magnetic layers in the sample. Also, we estimate the maximum current density as $\approx 10^4$ A/cm² for $I = 1$ mA through $1 \times 10 \mu\text{m}^2$ area near the Au lead, which is obviously not enough to create magnetization precession in a whole, $\approx 1 \mu\text{m}$ thick, Co₃Sn₂S₂ flake. The observed effects are not connected with contact effects, since they are observed in a four-point technique and are tested to be independent of the particular contacts. The bulk of the sample is fully spin-polarized⁸ above ≈ 0.5 T, see Fig. 2, so we can not attribute dV/dI spikes to any bulk spin structures like domains. Domains are always accompanied by hysteresis in $dV/dI(I)$ curves^{20,23}, which can not be seen in the inset to Fig. 3 (a).

However, we observe multiple magnon branches in Fig. 4 (a) at low, $\approx 10^4$ A/cm², current density, which requires some magnetic structure with small total spin S . On the other hand, apart from magnetically ordered bulk, broken time-reversal symmetry WSMs are characterized by topologically protected Fermi-arc surface states, which survive also in high magnetic fields. Due to the spin-momentum locking, they are characterized by complicated spin textures, which allows spin waves excitation^{14,15}.

Spin waves in the Weyl surface states well explain all the observed effects:

(i) We observe linear magnetic field dependence of the spikes' positions in in Fig. 4 (a), which well corresponds to the expected $I_{sw}(B)$ dependence. Low current density reflects the small total spin S in the narrow surface state, which is unreachable in traditional ferromagnetic multilayers.

(ii) Because of complicated spin and momentum structure¹, Weyl surface states support^{14,15} several spin-wave

excitation modes. Different modes are described by different fields H_{ex} and H_{an} , which is reflected in different onset current at zero magnetic field in Fig. 4 (a). As expected, different modes have the same $I_{sw}(B)$ slope, defined by S and the materials parameters, so all the branches are parallel in Fig. 4 (a).

(iii) Since the magnetic field affects the orbital motion of electrons in the surface state, high field creates reconstruction of spin textures due to the spin-momentum locking. We observe this reconstruction as the dV/dI spikes' interplay in high magnetic fields, see Fig. 4 (b).

To create the spin-wave excitations, one need the spin-polarized current from the ferromagnetic bulk to the surface states, somewhat similarly to magnetic multilayers²⁰⁻²⁶. In multilayers, the asymmetry of dV/dI spikes reflects the intrinsic asymmetry of spin diode with two non-equivalent ferromagnetic layers. In WSMs, the surface states cover all the sample surface, so one should observe dV/dI spikes for both current polarities for fully symmetric sample. The real Co₃Sn₂S₂ flakes are always strongly not symmetric, see Fig. 1 (a), which creates higher current density for one region of the sample and is responsible for the spikes asymmetry in Fig. 3.

V. CONCLUSION

As a conclusion, we experimentally investigate electron transport in kagome-lattice ferromagnet Co₃Sn₂S₂, which is regarded as a time reversal symmetry broken Weyl semimetal candidate. We demonstrate $dV/dI(I)$ curves with pronounced asymmetric dV/dI spikes, similar to those attributed to current-induced spin-wave excitations in ferromagnetic multilayers. In contrast to multilayers, we observe several dV/dI spikes' sequences at low, $\approx 10^4$ A/cm², current densities for a thick single-crystal Co₃Sn₂S₂ flake in the regime of fully spin-polarized bulk. The observed behavior necessarily requires a distinct magnetic structure with a small total spin value, so we attribute dV/dI spikes to multiple magnon branches in Co₃Sn₂S₂ Weyl surface states. We demonstrate splitting of the magnon branches in high magnetic fields, which may reflect reconstruction of spin textures in the surface state due to the spin-momentum locking. Presence of spin-transfer effects at low current densities in Co₃Sn₂S₂ makes the material attractive for applications in spintronics.

ACKNOWLEDGMENTS

We wish to thank V.T. Dolgoplov and Yu.S. Barash for fruitful discussions, and S.V. Simonov for X-ray sample characterization. We gratefully acknowledge financial support partially by the RFBR (project No. 19-02-00203), RAS, and RF State task.

-
- ¹ For a review on topological semimetals, see N.P. Armitage, E.J. Mele, and A. Vishwanath, *Rev. Mod. Phys.* **90**, 015001 (2018).
- ² P.K. Das, D.D. Sante, I. Vobornik, J. Fujii, T. Okuda, E. Bruyer, A. Gyenis, B.E. Feldman, J. Tao, R. Ciancio, G. Rossi, M.N. Ali, S. Picozzi, A. Yazdani, G. Panaccione, and R.J. Cava, *Nature Comm.* **7**, 10847 (2016).
- ³ B. Feng, Y.-H. Chan, Y. Feng, R.-Y. Liu, M.-Y. Chou, K. Kuroda, K. Yaji, A. Harasawa, P. Moras, A. Barinov, W. Malaeb, C. Bareille, T. Kondo, S. Shin, F. Komori, T.-C. Chiang, Y. Shi, and I. Matsuda, *Phys Rev B* **94**, 195134 (2016).
- ⁴ X. Wan, A. M. Turner, A. Vishwanath, S. Y. Savrasov, *Phys. Rev. B* **83**, 205101 (2011).
- ⁵ M. Hirschberger, S. Kushwaha, Z. Wang, Q. Gibson, S. Liang, C. A. Belvin, B. A. Bernevig, R. J. Cava, N. P. Ong, *Nat. Mater.* **15**, 1161-1165 (2016).
- ⁶ G. Xu, H. Weng, Z. Wang, X. Dai, Z. Fang, *Phys. Rev. Lett.* **107**, 186806 (2011).
- ⁷ S. K. Kushwaha, Z. Wang, T. Kong, R. J. Cava, *J. Phys. Condens. Matter* **30**, 075701 (2018).
- ⁸ Enke Liu, Yan Sun, Nitesh Kumar, Lukas Muechler, Aili Sun, Lin Jiao, Shuo-Ying Yang, Defa Liu, Aiji Liang, Qiunan Xu, Johannes Kroder, Vicky Süß, Horst Borrmann, Chandra Shekhar, Zhaosheng Wang, Chuanying Xi, Wenhong Wang, Walter Schnelle, Steffen Wirth, Yulin Chen, Sebastian T. B. Goennenwein, and Claudia Felser, *Nature Physics* **14**, 1125 (2018)
- ⁹ Qi Wang, Yuanfeng Xu, Rui Lou, Zhonghao Liu, Man Li, Yaobo Huang, Dawei Shen, Hongming Weng, Shancai Wang and Hechang Lei, *Nature Communications* **9**, 3681 (2018)
- ¹⁰ Noam Morali, Rajib Batabyal, Pranab Kumar Nag, Enke Liu, Qiunan Xu, Yan Sun, Binghai Yan, Claudia Felser, Nurit Avraham, Haim Beidenkopf, arXiv:1903.00509
- ¹¹ For a review on AHE, see N. Nagaosa, J. Sinova, S. Onoda, A.H. MacDonald, and P.P. Ong, *Rev. Mod. Phys.* **82**, 15391592 (2010).
- ¹² F. D. M. Haldane, *Phys. Rev. Lett.* **93**, 206602 (2004).
- ¹³ S. Nakatsuji, N. Kiyohara, and T. Higo, *Nature* **527**, 212215 (2015).
- ¹⁴ Jimmy A. Hutasoit, Jiadong Zang, Radu Roiban, and Chao-Xing Liu, *Phys. Rev. B* **90**, 134409 (2014)
- ¹⁵ Yasufumi Araki and Kentaro Nomura, *Phys. Rev. B* **93**, 094438 (2016)
- ¹⁶ O. O. Shvetsov, V. D. Esin, A. V. Timonina, N. N. Kolesnikov, and E. V. Deviatov *Phys. Rev. B* **99**, 125305 (2019)
- ¹⁷ A. Kononov, O.O. Shvetsov, S.V. Egorov, A.V. Timonina, N.N. Kolesnikov and E.V. Deviatov *EPL*, **122**, 27004 (2018)
- ¹⁸ O.O. Shvetsov, A. Kononov, A.V. Timonina, N.N. Kolesnikov, E.V. Deviatov, *JETP Letters*, **107**, 774779 (2018); *EPL*, **124**, 47003 (2018).
- ¹⁹ A. G. M. Jansen, A. P. van Gelder, and P. Wyder, *J. Phys. C* **13**, 6073 (1980)
- ²⁰ E.B. Myers, D.C. Ralph, J.A. Katine, R.N. Louie, R.A. Buhrman, *Science*, **285**, 867 (1999).
- ²¹ M. Tsoi, A. G. M. Jansen, J. Bass, W.-C. Chiang, M. Seck, V. Tsoi, and P. Wyder, *Phys. Rev. Lett.*, **80**, 4281 (1998).
- ²² M. Tsoi, A. G. M. Jansen, J. Bass, W.-C. Chiang, V. Tsoi and P. Wyder, *Nature*, **406**, 46, (2000).
- ²³ J. A. Katine, F. J. Albert, R. A. Buhrman, E. B. Myers and D. C. Ralph, *Phys. Rev. Lett.*, **84**, 3149 (2000)
- ²⁴ Y. Ji, C. L. Chien, and M. D. Stiles, *Phys. Rev. Lett.*, **90**, 106601 (2003)
- ²⁵ O. P. Balkashin, V. V. Fisun, I. K. Yanson, L. Yu. Triputen, A. Konovalenko, and V. Korenivski, *Phys. Rev. B*, **79**, 092419 (2009)
- ²⁶ T. Balashov, A. F. Takács, M. Däne, A. Ernst, P. Bruno, and W. Wulfhekkel, *Phys. Rev. B*, **78**, 174404 (2008)
- ²⁷ J.P. Eisenstein et al., *Phys Rev. B* **41** R7910 (1990); L.W. Engel et al., *Phys Rev. B* **45**, 3418 (1992); W. Kang et al., *Phys Rev. B* **56**, R12776 (1997).
- ²⁸ V. S. Khrapai, E. V. Deviatov, A. A. Shashkin, V. T. Dolgoplov, F. Hastreiter, A. Wixforth, K. L. Campman, and A. C. Gossard, *Phys. Rev. Lett.* **84**, 725 (2000).
- ²⁹ J.H. Smet, R.A. Deutschmann, et al., *Phys. Rev. Lett.*, **86**, 2412 (2001).
- ³⁰ J.C. Slonczewski, *J. Magn. Magn. Mater.* **159**, L1-L7 (1996).